Modeling Gait Variation Across People for Exoskeleton Control

José A. Montes Pérez, Gray Cortright Thomas, and Robert D. Gregg

Abstract— **Everyone walks differently. Exoskeletons depend on understanding a user's joint patterns to effectively synchronise the joint torques that they apply. Current exoskeletons are not designed to learn a user's joint patterns. Therefore, they have to make a trade-off between using a "one-size-fits-most" controller, and accepting the errors that comes with it, or having to manually tune the controller for each person. This work is centered on creating a data-driven, low-dimensional representation of individuals' joint patterns using principal component analysis (PCA), and then using it to estimate a new person's joint pattern in real time with an extended Kalman filter (EKF). Additionally, we test the hypothesis that a joint pattern model with less error will reduce synchronization error by fitting the low-dimensional representation to an individual, offline, using least squares. Our online and offline personalized gait model is compared with a "one-size-fits-most" model in a leave-one-out cross validation experiment to understand if the root mean squared error (RMSE) of the state of the EKF (which represent synchronization) is reduced. Running the experiment in silico using an able bodied dataset, we found that the offline personalized model reduced the phase and stride length estimated RMSE ($P<0.05$). However, the online personalized gait state model increased the RMSE of phase ($P<0.001$) and had similar performance for stride length ($P=0.774$).**

I. Introduction

Partial-assistance lower-limb exoskeletons have the potential to transform the mobility of humans by aiding in activities of daily life, such as walking, using stairs, and lifting heavy objects. They do this by supplying torques at the hips, knee, and ankle in the sagittal plane, which reduce the need for the activation of the user's own muscles. Studies have shown their capability to reduce the metabolic cost of walking [1]–[3]. However, to properly aid people, these systems must be synchronized with their human wearers. This is complicated by the fact that everyone walks differently.

Variations in how people walk introduce error in exoskeleton controls because their synchronization relies on predictions of the user's gait pattern. Synchronization algorithms that are meant to work in the real world can only use onboard sensors that measure joint angles, angular velocity, and linear acceleration in order to estimate the wearer's gait state [4]. Gait state are variables that allow the controller to determine what torque to apply. In this work it is defined as phase (stride completion percentage), the derivative of phase with respect to time (phase rate), and stride length.

Since human gait is periodic, it is possible to exploit that periodicity by creating models that are a function of the gait state. Sensors can then track these models to synchronize the exoskeleton's assistance to the user's current gait phase. However, the periodic pattern measured by the sensors depends on the person. Having an incorrect model can cause systematic errors in phase calculations, which leads to the incorrect torque being applied to the user. Incorrect torque can negate the positive assistive benefits of the exoskeleton and lead to discomfort, higher metabolic cost, and possible injuries to the user. Therefore, exoskeleton either need to understand the difference between people or be robust against those differences. Previous techniques have had some success on being robust, however, they mostly struggle to work outside of the laboratory.

The most common synchronization technique in the literature uses detected heel-strike events to predict future heel-strike events [4]. The phase estimate is based on the time until the next predicted heel-strike. For example, the duration of the previous stride could be used to linearly increase phase from 0 to 1 for the same duration during the next step. This is good for steady state walking such as in a laboratory setting, but it leads to uncomfortable transitions from walking to standing and vice versa. The main drawback of this method is that the phase rate estimations are always one step behind the users current intent, limiting field applicability.

Synchronization has also been approached using adaptive oscillators [5]–[7], which are nonlinear dynamical systems that converge to tracking any periodic signal. Their key ability to detect patterns has also proven useful for removing periodic delay biases from pose estimating filters when operating on periodic behavior like walking [8]. However because they focus on patterns, the approach struggles with sudden changes in gait type (different walking speeds, slopes, stairs, etc.), and the states of the filter do not necessarily give information about the current task (e.g. estimating ground inclination), even when that information is key to applying the right assistance (e.g. more torque for steeper slopes).

An emerging approach to synchronization builds on the adaptive oscillator concept by applying an extended Kalman filter (EKF) to track periodic motion [9], [10]. The EKF's state corresponds to the gait state and the oscillating behavior is represented by the dynamics of the state estimator's model. The state estimator's model can also leverage continuously parameterized "general gait models" as introduced in [11]. By doing this, the estimator can additional infer the task-variables of the locomotion task such as phase rate, stride length, and ground inclination [9]. However, such approaches are inherently sensitive to the quality of the gait model. Their performance suffers when models trained for the average person are applied to gait containing individual variation.

When comparing sources of error in models of joint kinematics, personal gait differences are the largest contributors to lower-limb angle error during walking on level ground and ramps [12]. Therefore, individualized models of joint kinematics vastly improve the quality of their predictions.

Therefore, our hypothesis is that having a personalized model will increase the prediction accuracy of the gait state estimator. But estimating completely personalized gait models would require an excessive data collection for each new person. This is fundamental to the high dimensionality of the gait model and therefore the personalized gait model. Such a high-dimensional model is necessary to express the gait patterns of multiple sensors continuously over multiple activities. But at the same time this high dimensionality in the parameters requires a comparable quantity of training data to learn an entirely new model for each person.

A common way of simplifying high dimensional systems is by performing principal component analysis (PCA) to approximate the most salient parts with a lower-dimensional system. This technique can, for example, decompose pathological gait into the most prominent types of compensation [13]–[15]. It can also decompose data-sets of coordinated whole body motion into the fundamental different types of people, and then use this to identify people from their motion [16].

In this paper, we create a gait estimation system that estimates phase, phase rate, stride length, and a low-dimensional representation of the user's joint kinematics, which we call a "gait fingerprint". The most important differences across people's joint kinematics were found by fitting models to able bodied walking data, and performing PCA on the set of fits. This PCA is performed in a specially constructed vector space to ensure that down-selection is performed in units of RMSE changes to the gait model. The output of the PCA is defined as the 'personalization map'. An EKF then uses the personalization map is to estimate the individuals joint kinematics alongside estimating the current gait phase. This online-learned model is denoted as the gait-fingerprint model (GF). In addition to the online model, an offline, low-dimensional model is calculated for an individual by performing least squares with the personalization map on the individual's pre-recorded data. This least squares, gait fingerprint (LS-GF) model is used to test that the personalization map can generate meaningful improvements in model fit and see if models with lower RMSE generate better gait state tracking. We validate the algorithm with leave-one-out cross validation for the subjects in an able-bodied dataset [17]. The performance is compared against the baseline approach [9] that uses a inter-subject average (AVG) model to approximate new individuals. Our metrics center on root mean squared error (RMSE) of the predicted gait states, which relate to our intended application in synchronization and adaptation of exoskeleton controllers to personalized human gait across multiple tasks.

II. Gait State Estimator

The gait state estimator is the algorithm that will calculate the gait state (phase, and task variables), and individualized joint kinematics. Our implementation is based on an extended Kalman filter which predicts the gait state and personalized kinematics from thigh angle and angular velocity measurements. However, this method can easily be expanded by the adding additional joint angle and velocity measurements. The following derivation is done with multiple joints in mind.

A. Gait Dynamics

We define our gait-state vector as

$$x(t) = \begin{bmatrix} p(t) & \dot{p}(t) & l(t) & g_1(t) & \dots & g_{n_g}(t) \end{bmatrix}^T, \quad (1)$$

where p, is the phase variable, $\dot{p}$ is the rate of change of phase with respect to time (phase rate), and l represents stride length. The remaining elements, $g_1(t)$ through $g_n(t)$, are the gait fingerprints. Phase is bounded in $[0, 1)$

These states follow simple dynamics. Phase integrates phase rate, and the remaining states evolve independently of each other, simply integrating independent process noise. The process model is then:

$$x_{k+1} = Fx_k + \omega_Q, \quad \omega_Q \sim \mathcal{N}(0, \Sigma_Q), \quad (2)$$

in terms of matrices F and Σ_q with

$$F = \begin{bmatrix} 1 & \Delta t & \\ & 1 & \\ & & I_{n_g+1} \end{bmatrix}, \; \Sigma_Q = \begin{bmatrix} \sigma^2_{Q,1} & & \\ & \ddots & \\ & & \sigma^2_{Q,n_g+3} \end{bmatrix}, \quad (3)$$

where n_g is the number of gait fingerprints, ω_Q is a multivariate normal with mean 0 and Σ_Q covariance, I_{n_g+1} is an $n+1$ dimensional identity matrix, and Δt is the time-step.

B. Measurement Model

Our measurement model predicts a suite of sensor signals using the gait state. We define the number of joint angle measurements as m. The number of total signals, including the velocities is then $2m$. We denote the measurement model as

$$z(t) = h(x(t)) + \omega_R, \quad \omega_R \sim \mathcal{N}(0, \Sigma_R), \quad (4)$$

where $z(t)$ is the measurement at time t, $h(x(t))$ applies the measurement model, $h(\cdot)$, to the state, $x(t)$, to obtain a noiseless measurement, and noise ω_R comes from a multivariate normal distribution $\mathcal{N}(0, \Sigma_R)$ with mean 0 and covariance Σ_R, defined as

$$\Sigma_R = \text{diag}\left(\begin{bmatrix} \sigma^2_{R,1} & \dots & \sigma^2_{R,m} \end{bmatrix}\right), \quad (5)$$

where 'diag' constructs a diagonal matrix.

Our model of the expected joint angles and joint velocities is as follows:

$$\theta_j = \Lambda(p, \dot{p}, l)\xi_j(g), \quad (6)$$

where $\Lambda \in \mathbb{R}^{1\times c}$ is a row vector function of functions that define a basis shared between all subjects, and $\xi_j(\cdot)$ is a function that maps subject specific gait fingerprint vector $g = \begin{bmatrix} g_1(t) \dots g_{n_g}(t) \end{bmatrix}^T$ to a $c \times 1$ column vector that represents the subject-specific joint kinematics. However, since the measurement model consist of the global foot angle,

global shank angle and the global thigh angle, then these are concatenated as follows:

$$\theta = \overbrace{\begin{bmatrix} \Lambda(x) & & \\ & \Lambda(x) & \\ & & \Lambda(x) \end{bmatrix}}^{\Lambda_\theta(x)} \overbrace{\begin{bmatrix} \xi_1(g) \\ \vdots \\ \xi_m(g) \end{bmatrix}}^{\xi(g)} = \Lambda_\theta(x)\xi(g), \quad (7)$$

where each joint has the same basis functions and only vary by the fit, ξ_j, which defines the kinematics for a particular joint and person. Joint velocity is calculated by differentiating the model with respect to time:

$$\dot{\theta} = \overbrace{\begin{bmatrix} \frac{\partial \Lambda(x)}{\partial p}\dot{p} & & \\ & \frac{\partial \Lambda(x)}{\partial p}\dot{p} & \\ & & \frac{\Lambda(x)}{\partial p}\dot{p} \end{bmatrix}}^{\Lambda_{\dot{\theta}}(x)} \xi(g) = \Lambda_{\dot{\theta}}(x)\xi(g), \quad (8)$$

Here we use the same fit as the joint but multiply it by Λ differentiated with respect to time, a relationship we get through the chain rule.

Therefore the total measurement model is defined as

$$h(x) = \begin{bmatrix} \Lambda_\theta(x) \\ \Lambda_{\dot{\theta}}(x) \end{bmatrix} \xi(g). \quad (9)$$

Finally, $\xi(g)$ is defined as

$$\xi(g) = \xi_{\text{avg}} + P_{\text{map}} g, \quad (10)$$

where the matrix P_{map} is the personalization map and defines the relationship between the gait fingerprint vector and the subject-specific gait model parameters, and ξ_{avg} defines the average model parameters among the subjects. The average model parameters are defined Sec. III-A and the P_{map} is derived in Sec. III-C.

C. Kronecker Model Definition

The function basis $\Lambda(x)$ is defined using the Kronecker product ($\otimes$) of simpler function bases, as

$$\Lambda(p, \dot{p}, l) = \lambda_1(p) \otimes \lambda_2(\dot{p}) \otimes \lambda_3(l) \quad (11)$$

where each λ_i is a row basis function, such as the first few elements of a Fourier series of powers of a polynomial, and $\otimes$ represents the Kronecker product operation. In this work, the Kronecker product is used to generate every linear combination of the different elements of each basis function. As an example, given two matrices $A \in \mathbb{R}^{1\times\alpha_1}$ and $B \in \mathbb{R}^{1\times\alpha_2}$, the resulting Kronecker product will be $A \otimes B \in \mathbb{R}^{1\times(\alpha_1\alpha_2)}$. The math used in this section is independent of any particular size of model. The generalized Kronecker product is described in [18].

For the measurement model in equation (11), the basis functions are defined as a Fourier series or Taylor series. The Fourier basis of order k is defined as $F_k(x) = \begin{bmatrix} 1 & \sin(x) & \cos(x) & \dots & \sin((k-1)x) & \cos((k-1)x) \end{bmatrix}$, and the polynomial basis of order k is defined as $P_k(x) = \begin{bmatrix} x^0 & \dots & x^{k-1} \end{bmatrix}$. For the validation experiments, the basis are defined as fourth order Fourier basis in phase, and first order polynomial in phase rate, and a second order polynomial in stride length.

III. Personalization Map

A. Differences from the Average Gait

The goal of the personalization map is meant to describe the differences is how people walk. To understand the most important differences from the average gait, first, we need to define how to talk about an individual's gait in order to understand what the average gait is, and then calculate differences from the average. The model for all the joint angles is defined in (7). Since the problem is over-constrained, to calculate the fit for a particular subject, least squares is used as follows

$$\theta_q = \Lambda_q \xi_q, \quad (12)$$

$$\xi_q = (\Lambda_q^T \Lambda_q)^{-1} \Lambda_q^T \theta_q. \quad (13)$$

Here, θ_q is a $mN_q \times 1$ vector that represents the measured joint angles for person q in the dataset, Λ_q is a $mN_q \times mc$ matrix defined as $\Lambda_\theta(x)$ evaluated with all the corresponding states, and ξ_q is an $mc \times 1$ vector that encodes the individual characteristics of a person's gait.

Therefore, to calculate the average person's gait, the fits for all the subjects are averaged

$$\xi_{\text{avg}} = \frac{1}{n_q} \sum_{q=1}^{n_q} \xi_q. \quad (14)$$

Where n_q represents the amount of subjects in the dataset. After having obtained the average fit, then the difference from the average for all the people is defined as the subtraction of the average from the individual's fit. These are aggregated into a matrix that has the differences between all the subjects in the dataset and the average gait:

$$\Xi_0 = \begin{bmatrix} \xi_1 - \xi_{\text{avg}} & \dots & \xi_{n_q} - \xi_{\text{avg}} \end{bmatrix}. \quad (15)$$

B. Change of Basis into Joint-RMSE Space

Eq. (15) could be used to perform dimensionality reduction via principal component analysis (PCA), however, this technique is dependent on the scaling of each vector. Therefore, to obtain meaningful features we introduce a change of basis into an 'RMSE' vector space. That is, vectors in this space have L2-norms that correspond to the root mean square error (RMSE) in measurement units of the measurement models they imply. This will normalize the values across all the joints to have comparable 'units' and therefore extract features from the PCA algorithm that impact RMSE.

We begin the development of the change of basis by defining an inner product for vector valued functions,

$$\langle f_1, f_2 \rangle_f = \frac{\int_{x\in\mathcal{X}} \rho(x) f_1^T(x) f_2(x) dx}{\int_{x\in\mathcal{X}} \rho(x) dx} \quad (16)$$

where $\mathcal{X}$ represents the entire space of the state, $\rho(x)$ is a density function representing a weighting over the states. This inner product over function spaces, $< \cdot, \cdot >_f$, induces

an inner product over parameter vectors ξ, $< \cdot, \cdot >_\xi$, as

$$\begin{aligned}\langle \xi_1, \xi_2 \rangle_\xi &= \langle \Lambda(x)\xi_1, \Lambda(x)\xi_2 \rangle_f, \\ &= \frac{\int_{x\in\mathcal{X}} \rho(x)\xi_1^T \Lambda_\theta^T(x)\Lambda_\theta(x)\xi_2 dx}{\int_{x\in\mathcal{X}} \rho(x)dx}. \end{aligned} \tag{17}$$

This inner product is defined in terms of a density function $\rho(x)$, which requires integration. However, if we equally weight every state that was observed during any task and any subject in our dataset (restricted to level ground walking), we can simplify this to a summation. This assumption makes the density function $\rho(x) = \sum_{x_i\in\mathcal{D}} \delta(x_i)$, where $\delta(\cdot)$ is the Dirac delta function, $\mathcal{D}$ is the training set which includes different subjects, and x_i is the state in the is $\mathcal{D}$. With this definition of $\rho(x)$, the integral simplifies to

$$\langle \xi_1, \xi_2 \rangle_\xi = \sum_{x\in\mathcal{D}} \frac{\xi_1^T \Lambda_\theta(x)^T \Lambda_\theta(x)\xi_2}{N_\mathcal{D}}, \tag{18}$$

$$\langle \xi_1, \xi_2 \rangle_\xi = \xi_1^T \underbrace{\frac{\sum_{x\in\mathcal{D}} \Lambda_\theta(x)^T \Lambda_\theta(x)}{N_\mathcal{D}}}_{G} \xi_2, \tag{19}$$

$$\langle \xi_1, \xi_2 \rangle_\xi = \xi_1^T G \xi_2, \tag{20}$$

where positive definite G is defined as the approximate Gram matrix of Λ. By evaluating all the data for every individual, we hope to approximate the structure. The resulting inner product can now be used to understand the difference between two fits.

This inner product is then used to define a desired basis as follows:

$$\theta = \Lambda_\theta \xi = \hat{\Lambda}_\theta \xi^{'} \tag{21}$$

$$\hat{\Lambda}_\theta = \begin{bmatrix} \lambda_1^{'} & \dots & \lambda_o^{'} \end{bmatrix}, \text{ s.t. } \langle \lambda_i^{'}, \lambda_j^{'} \rangle_f = \begin{cases} 1, & \text{when } i = j \\ 0, & \text{when } i \neq j \end{cases}$$

Here, the basis $\hat{\Lambda}$ defines a different ordering and/or combination of the same basis functions that are in Λ, however, with the property that the l2-norm on the corresponding $\hat{\xi}$ vector equates to a change in degree RMSE of the same magnitude. The change of basis to go into the orthonormal space $\hat{\Lambda}$ is defined as follows:

$$\theta = \Lambda_\theta Q Q^{-1} \xi = \hat{\Lambda}_\theta \hat{\xi} \tag{22}$$

$$\hat{\xi} = Q^{-1}\xi, \quad \hat{\Lambda}_\theta = \Lambda_\theta Q, \quad Q^{-1} = Q^T,$$

where Q is a square $mc \times mc$, invertible matrix that represents the change of basis for a particular joint. To calculate Q we note the following:

$$\hat{G} = \frac{\int_{x\in\mathcal{X}} \rho(x)\hat{\Lambda}^T(x)\hat{\Lambda}(x)dx}{\int_{x\in\mathcal{X}} \rho(x)dx}, \tag{23}$$

$$= \sum_{x\in\mathcal{D}} \frac{Q^T \Lambda_\theta(x)^T \Lambda_\theta(x) Q}{N_\mathcal{D}}, \tag{24}$$

$$= Q^T G Q = I. \tag{25}$$

Here, G is the same as defined above. As a second step to calculate Q, perform the eigenvalue decomposition on G, $G = O^T V O$. Then, the matrix Q is defined as

$$Q = O V^{\frac{-1}{2}} O^T. \tag{26}$$

This can be proved as follows:

$$I = Q^T G Q = Q^T (O^T V O) Q, \tag{27}$$

$$= (O^T V^{-\frac{1}{2}} O)(O^T V O)(O^T V^{-\frac{1}{2}} O), \tag{28}$$

$$= O^T V^{-\frac{1}{2}} V V^{-\frac{1}{2}} O = O^T O = I. \tag{29}$$

Therefore, using the data used to generate the subject fits we have been able to find the change of basis function into the "RMSE" space.

C. Personalization Map Definition

Combining the results from the past two sub-sections, we get the matrix of fits in RMSE space:

$$\Xi_{0,RMSE} = \Xi_0 Q^{-1}. \tag{30}$$

To reduce the dimension of the system, principal component analysis was used. That is, the covariance matrix

$$\Xi_{cov} = \frac{\Xi_{0,RMSE}^T \Xi_{0,RMSE}}{n_q - 1}, \tag{31}$$

is calculated and then the eigenvalue decomposition of the matrix is performed:

$$\Xi_{cov} = U^T \Psi U, \tag{32}$$

$$\Psi = \text{diag}\left(\begin{bmatrix} \psi_1 & \dots & \psi_{n_q} \end{bmatrix}\right), \tag{33}$$

where $\psi_1 > \psi_2 > \cdots > \psi_{n_q}$ represent the principal components of the matrix.

To determine the amount of vectors of U that will make up the personalization map two things will be considered: maximizing the variance observed across the subjects, and minimizing the amount of vectors to minimize the states that are added to the Kalman filter. The threshold set for the variance explained is 99% of the observed data in $\Xi_{0,RMSE}$. The second consideration is added given that the computation complexity of the extended Kalman filter is $\mathcal{O}(s^3)$. To calculate the variance observed, we use the following:

$$\text{Var}_{\text{obs}} = \frac{\sum_{i=1}^{n_g} \psi_i}{\sum_{i=1}^{n_q} \psi_i} \tag{34}$$

where n is an integer and is selected to be the smallest value such that $\text{Var}_{\text{obs}} > 0.99$. Therefore, the personalization map is defined as

$$P_{\text{map}} = U^T \text{diag}\left(\begin{bmatrix} \psi_1 & \dots & \psi_{n_g} & \dots & 0 \end{bmatrix}\right) U \tag{35}$$

D. Learning the Gait-Fingerprints from Data

In order to understand what the optimal gait fingerprints are for a person (LS-GF model), we can modify (12) to replace ξ_q with $\xi(g_q)$ (the least squares version of the gait

fingerprint for person q), and then calculate g_q via least squares:

$$\theta_q = \Lambda_q \xi(g_q), \tag{36}$$

$$\theta_q = \Lambda_q(\xi_{\text{avg}} + P_{\text{map}} g_q), \tag{37}$$

$$\underbrace{\theta_q - \Lambda_q \xi_{\text{avg}}}_{\theta'} = \underbrace{\Lambda_q P_{\text{map}}}_{\Lambda'} g_q, \tag{38}$$

$$\theta' = \Lambda' g_q, \tag{39}$$

$$g_q = (\Lambda'^T \Lambda')^{-1} \Lambda'^T \theta'. \tag{40}$$

IV. Experimental Setup

A. In-Silico Testing

To validate that our method is better at tracking the gait state for subjects it has not seen before in-silico leave-one-out cross-validation was used based on an able-bodied walking dataset [17].

Since there are 10 subjects in the dataset, the leave-one-out cross-validation experiment consisted of using nine subjects to train the personalization map and average fit. In the baseline comparison, we use our own basis models and not the ones from [9] to calculate the inter-subject average. The LS-GF was fit by feeding in the ground truth for the left-out-subject. All the methods will be initialized with the same initial state and covariance, however, the process noise for each will be tuned independently for each method to ensure that optimal performance for each method can be achieved. To validate that the EKF can estimate the new subject's joint kinematics, the gait fingerprints will be initialized to be zero. This corresponds to starting in the 'average person' and then converging into the specific person. The results of each trial will be compared by calculating the RMSE error for each of the states.

B. Measurement Model Covariance Tuning

For each leave-one-out validation test, the measurement covariance matrix Σ_R will be tuned so that the diagonal entries corresponding to each joint are set to the average of the squared residual for each training subject:

$$\sigma^2_{R,\text{thigh}} = \frac{1}{n_q} \sum_{q=1}^{n_q} \frac{|\theta_q - \Lambda_q \xi_q|}{N_q}. \tag{41}$$

Since in this case we just have one angle, then

$$\Sigma_R = \sigma^2_{R,\text{thigh}}. \tag{42}$$

C. Process Model Covariance Tuning

The tuning of the process model noise Σ_Q was done by iterative hand tuning based on the observation of the in-silico testing results. Increasing the values of $\sigma^2_{Q,i}$ increases the time response of state number i. Since the measurement model is fixed, this is the 'knob' that allows us to determine how states change relative to one another. Phase rate and stride length share similar changes in magnitude in the data, therefore, their process model noise components were tuned so that they had a similar order of magnitude. Since phase is calculated by the forward integration of phase rate, the noise model component of phase is zero. The gait fingerprint's process model noise is tuned such that they converge at a reasonable rate, without interfering with the other states. Additionally, since the gait fingerprints are not present in the inter-subject average model and least squares gait fingerprint models, and they have the same measurement noise, these will have a different process model noise to account for the higher frequency components. For the online gait fingerprint method, the phase rate noise was 9×10^{-8}, stride length noise was 6×10^{-8} and the gait fingerprint noise model was 4×10^{-10} for each of the gait fingerprints. In the inter-subject average model and least squares gait fingerprint model, the phase rate noise was 2×10^{-8}, stride length noise was 7×10^{-8}.

D. Validation Metrics

To quantify the performance of each method, we will use the root mean squared error (RMSE) of the predicted state versus the actual state from the dataset. It is calculated as the square root of the average squared error between the predicted state vector and the actual state vector for all data points in some dataset (training or validation).

The RMSE calculation for phase requires special consideration due to the discontinuous behavior near the end of the step . At this point, phase jumps from one to zero. If the prediction is leading or lagging by a small amount near the discontinuity then it will lead to large errors of phase when in reality they are close to each other. Therefore, to account for this error, the error between the actual phase and the predicted phase is $\min(|p - p'|, |1 - |p - p'|\,|)$. This means that if the error is too large, then it is most likely coming from the discontinuity, and therefore the true error can be found by subtracting one.

The RMSE error for each state, person, and method will be calculated (Tab. III). To determine which method is better, the average RMSE across all subjects will be calculated for each mean. If a subject does not converge for any of the methods, then it will not be included in the mean calculations. A t-test will be then computed to determine if each mean is significantly different when taking into account the variance of the difference. To determine if one method is better than another the one-sided t-test is used. If we are trying to compare if two things have similar performance, we will use the two-sided t-test.

E. Data Playback Considerations

The fact that pre-recorded data is used caused some artifacts that needed to be addressed to ensure proper operation of the extended Kalman filter. First, the dataset lacked joint angle velocities, which required to compare to the expected measurements. Therefore, they where added by numerically differentiate joint angles.

Additionally, when transitioning between different walking speeds there was no data for the intermediary steps. This means that there was a sharp change in conditions that might not be apparent with real world usage. In the transition of steps there will be discontinuities in joint angles

and joint velocities. This can cause the extended Kalman filter to "get lost" and not recover. To mitigate this impact, the measurement covariance corresponding to global thigh angle was increased by a factor of 2 and the covariance corresponding to global thigh angle velocity was increased by a factor of 10 when the estimated phase was higher than 0.95 and lower than 0.05. The joint angle velocity is penalized more due to the high velocities that occur due to discontinuities in the dataset. Additionally, the speeds where only transitioned to their nearest neighbor to minimize the magnitude of the discontinuity (e.g. belt speeds of 0.8m/s only transition to 1.0m/s and not to 1.2m/s).

V. Results

A. Determining Number of Gait Fingerprints

Given that there are multiple leave-one-out cross validation test, the selection of the gait fingerprints was based on the average variance observed across all the tests different test performed. It was observed that, on average, 3 gait fingerprints described more than 99% of the variance observed (Tab. I). Therefore, the number of gait fingerprints was chosen to be 3.

TABLE I
CUMULATIVE VARIANCE EXPLAINED BY GAIT FINGERPRINTS

Left-Out Subject	g_1	g_2	g_3
AB01	0.96%	0.98%	0.99%
AB02	0.97%	0.99%	0.99%
AB03	0.97%	0.99%	1.0%
AB04	0.95%	0.98%	0.99%
AB05	0.97%	0.99%	1.0%
AB06	0.97%	0.99%	1.0%
AB07	0.97%	0.99%	0.99%
AB08	0.97%	0.99%	0.99%
AB09	0.97%	0.99%	0.99%
AB10	0.98%	0.99%	1.0%

B. Model Fitting Results

The baseline model using the inter-subject average generated higher RMSE errors when comparing the error of the model predictions against the data when compared with the least squares calculated gait fingerprint (LS-GF) (Tab. II). This can be seen in Fig. 2 as the blue line (representing the LS-GF fit) fits the user data much closer.

TABLE II
PERSONALIZED LEAST SQUARES MODEL FITS

Left-Out Subject	Average RMSE	LS-GF RMSE	g_1	g_2	g_3
AB01	20.4	4.22	-19.4	-0.203	0.285
AB02	8.23	2.83	-7.525	-1.404	-1.562
AB03	3.52	3.15	0.537	-0.001	1.61
AB04	25.1	3.51	-26.0	-2.76	-0.956
AB05	8.64	4.06	8.038	0.0357	0.855
AB06	10.1	3.34	9.24	-1.28	0.548
AB07	8.39	4.47	6.96	2.16	2.02
AB08	16.2	4.5	-15.8	-2.58	-1.15
AB09	6.6	2.88	-5.54	1.79	-0.00742
AB10	4.17	3.17	-0.565	1.62	-2.54

C. Simulation Results

The results of each of the leave-one-out validation can be seen in Table III. The mean calculation excludes the data for AB10 since it was not possible to make the average model fit track the states without converging to the ground truth state, which resulted in higher than expected state RMSE.

The LS-GF model outperformed the inter-subject average model in phase and stride length ($P<0.5$). The online GF estimation method outperformed stride length calculations for 6 out of the 9 valid tests, however, it was not found to be statistically significant ($P=0.774$). The online GF method was worse at estimating phase ($P<0.001$).

VI. Discussion

A. Interpretation of Personalization Map

Each gait fingerprint describes one way the thigh angle pattern changes between the ways different people walk. While the variation is hard to describe across all speeds and stride lengths, the trends at a fixed stride length of 1.0 m and phase rate of 1.0 stride/s offer some more visualizable intuition (Fig. 1). At these conditions, the first gait fingerprint parameter appears to add a constant offset to predictions of thigh angle (Fig. 1.A). This first fingerprint takes large values when fit using least squares, up to 26 degrees RMSE (Tab. II). The second fingerprint takes smaller values, up to 2.76 degrees RMSE, and varies the magnitude of maximal hip extension and the timing of the timing of maximal flexion (Fig. 1.B). The third fingerprint is also small, taking values up to 2.54 degrees RMSE, and allows for a shift in the timing of peak hip flexion that corresponds to a change in peak extension magnitude that is opposite of the change offered by gait fingerprint 2.

The first gait fingerprint resembles a constant bias, and this suggests an interpretation as a sensor bias. The dataset recorded human kinematics using a Vicon motion capture system, for which the marker placement has a clear influence on the angular measurements. In particular, the pelvis position markers on the anterior superior illiac spine and posteriror superior illiac spine must be identified by palpation and are difficult to accurately determine. This could potentially introduce subject-specific biases into pelvis

TABLE III
RESULTS OF THE RMSE DURING THE LEAVE-ONE-OUT CROSS VALIDATION EXPERIMENTS

Left-Out Subject	Method	Phase*	Phase Rate*	Stride Length*
Mean	GF	0.0259††	0.0431††	0.1043
Mean	AVG	0.0189	0.0232	0.1122
Mean	LS GF	0.0170†	0.0227	0.0780†

GF — gait fingerprint method; AVG — baseline average method; LS GF — least squares gait fingerprint method; † — less than AVG condition, $P<0.05$; †† — greater than AVG condition, $P<0.001$; * — RMSE error; ♯ – test that did not properly converge to the ground truth state.

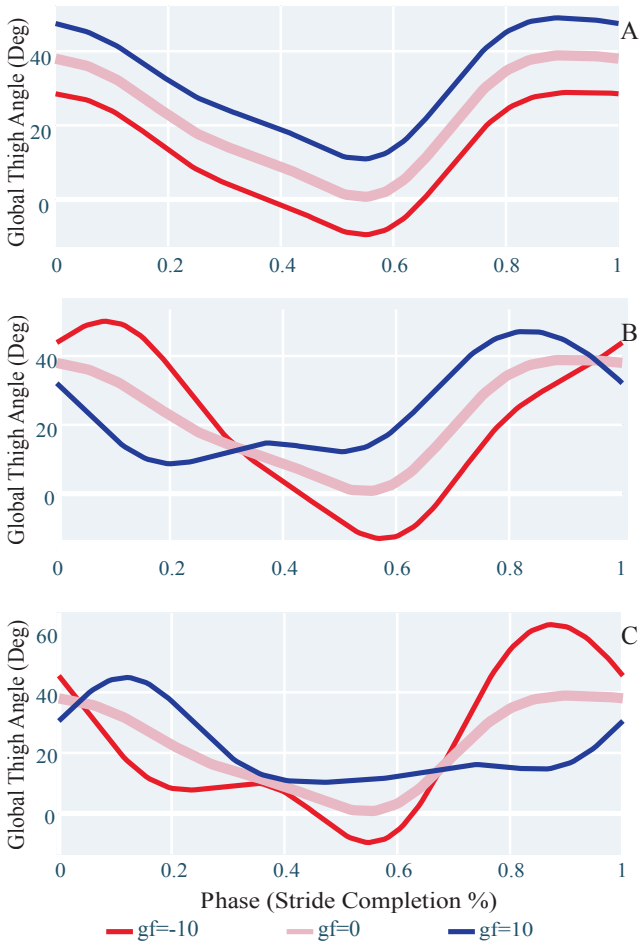

Fig. 1. Comparison of the inter-subject average (Pink) against ± 10 of one gait fingerprint. The top graph corresponds to the most important feature in the personalization map (g_1), the middle graph corresponds to the second most important feature (g_2), and the bottom corresponds to the third most important feature (g_3).

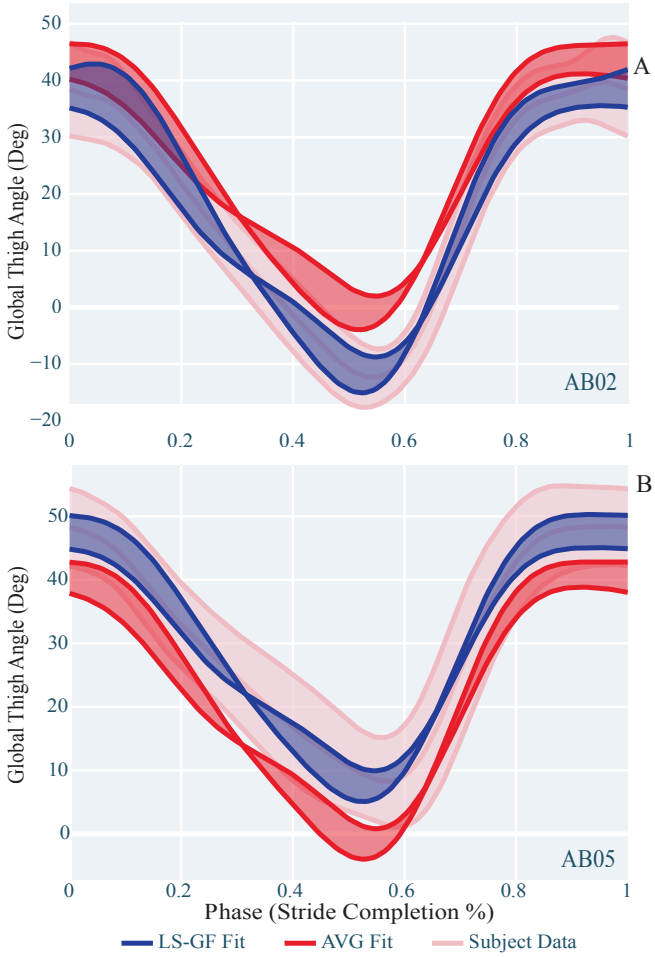

Fig. 2. Comparison of the mean $\pm$ 2 standard deviations for AB02 and AB05 data (pink) in comparison with the mean $\pm$ 2 standard deviations of the inter-subject average model (red) vs the personalized model (blue). Standard deviation calculations are done with respect to phase. AB05's data is close to the inter-subject average while AB02's data is not closely tracked by the inter-subject average fit. Both approximate the data better with the least squares gait fingerprint model.

angle measurements. A similar mechanism could bias global thigh angle measurements. However magnitudes on the order of 26 degrees seem too large to attribute them to marker placement alone. A biomechanical explanation could be that some subjects walked with varying degrees of bent knees during stance, which could also introduce a thigh angle bias.

The utility of our personalization map is partly tied to the sensor system on which it was generated. From the point of view of our system, the origin of this thigh angle bias cannot be determined. If some device were to be controlled using Vicon-based measurements of global thigh angle, the inclusion of the first gait fingerprint in the model would improve tracking performance in the same way for either underlying origin. The distinction would only appear when trying to port a model from one sensing system to another one—for example an exoskeleton system with only on-board sensing. In this case, aspects of sensor calibration unique to the new sensors would impede accurate sensor predictions, and aspects of the personalization model that were unique to the original sensors would be potentially made irrelevant. Thus to develop a truly sensor independent personalization map, more data from different sensors or formal guarantees on the quality of the dataset's sensors would be needed.

B. *Interpretation of Simulation Results*

While the fitting results showed that gait fingerprinting generated more accurate models (Table II), these results did not translate to improved real-time state estimates in genera (Table II). Models personalized by least squares estimation of the optimal gait fingerprints showed improved stride length performance [needs T-test].

The gait fingerprints in our EKF simulation did not appear to converge toward the least squares optimal fit, and there are several potential explanations for this. First, the gait fingerprint states changed on a relatively fast time scale as compared to the gait fingerprints that were fit by least squares. While the least squares problem considered gait fingerprints that were constant for the entirety of the dataset, the gait fingerprints learned online were able to adjust to

the individual walking activities at hand. This allowed them to respond to changes in task, which they did. Second, the gait fingerprints learned online interfered with the estimation of the other parameters. Gait fingerprints in the GF-LS condition were optimized according to ground truth stride length and phase information, whereas gait fingerprints in the EKF condition were optimized according to the live estimate of theses states.

Looking again at the gait fingerprint definitions (Fig. 1), it appears possible that the root cause of the increased errors in phase and stride length tracking from AVG to EKF conditions is related to the potential ability of gait fingerprints to shift the predicted angle trajectories in a way that can be confused with a change in phase or stride length. Qualitatively, it was observed that the gait-fingerprint method would struggle determining whether to change a gait-fingerprint or a state. This leads us to believe that there could be pairs of state and gait-fingerprints that look similar. It may be possible in the future to constrain the definition of the gait fingerprints to fall within a "nullspace" of the behaviors already permitted by adjusting phase and stride length, and thereby reduce this potential for incorrect state estimates.

Subjects that are close to average person will not receive much benefit from the average. This can be observed by looking at a subjects data and their corresponding model predictions. For example, AB05 did not improve with the LS-GF method, and looking at the data it can be seen that the inter-subject average model and the LS-GF model are very similar (relatively small g_2 and g_3). However, the inter-subject average model's prediction does not closely follow subject AB02's data (relatively big g_2 and g_3 in Table II). Additionally, it can be observed that it does have improvement in stride length and phase tracking.

The overall personalized EKF approach could reasonably be expected to scale to more sensor and state components according to the scaling of the EKF in general. The EKF approach also scales in the sense that it does not rely on any hand tuning by clinical professionals in order to track gait. However, to mitigate problems of confusion between fingerprints and task variables, it is possible to employ alternative strategies in the clinic in which the system is first trained and then locked. This can be seen as reduced data least squares (with the data split into training, personalizing, and validating).

C. Limitations

Perhaps the most important limitation of this approach is its reliance on the kinematic data from many participants. Tasks outside the trained tasks have no guarantees, and this is even further emphasized with the gait fingerprint parameters. With respect to a task outside our training data, we can not expect the gait fingerprints to be more helpful than randomly chosen replacements. The dependence of data is especially important for dealing with pathological gait, which would necessitate a database of pathological kinematics over various activities.

REFERENCES

[1] L. M. Mooney, E. J. Rouse, and H. M. Herr, "Autonomous exoskeleton reduces metabolic cost of human walking during load carriage," *Journal of NeuroEngineering and Rehabilitation*, vol. 11, no. 1, p. 80, May 2014. [Online]. Available: https://doi.org/10.1186/1743-0003-11-80

[2] M. Shepertycky, S. Burton, A. Dickson, Y.-F. Liu, and Q. Li, "Removing energy with an exoskeleton reduces the metabolic cost of walking," *Science*, vol. 372, no. 6545, pp. 957–960, 2021.

[3] S. Galle, P. Malcolm, S. H. Collins, and D. De Clercq, "Reducing the metabolic cost of walking with an ankle exoskeleton: interaction between actuation timing and power," *Journal of NeuroEngineering and Rehabilitation*, vol. 14, no. 1, p. 35, Apr 2017. [Online]. Available: https://doi.org/10.1186/s12984-017-0235-0

[4] R. Baud, A. R. Manzoori, A. Ijspeert, and M. Bouri, "Review of control strategies for lower-limb exoskeletons to assist gait," *Journal of NeuroEngineering and Rehabilitation*, vol. 18, no. 1, p. 119, Jul 2021. [Online]. Available: https://doi.org/10.1186/s12984-021-00906-3

[5] R. Ronsse, N. Vitiello, T. Lenzi, J. van den Kieboom, M. Chiara Carrozza, and A. J. Ijspeert, "Adaptive oscillators with human-in-the-loop: Proof of concept for assistance and rehabilitation," in *2010 3rd IEEE RAS EMBS International Conference on Biomedical Robotics and Biomechatronics*, 2010, pp. 668–674.

[6] K. Seo, S. Hyung, B. K. Choi, Y. Lee, and Y. Shim, "A new adaptive frequency oscillator for gait assistance," in *2015 IEEE International Conference on Robotics and Automation (ICRA)*, 2015, pp. 5565–5571.

[7] G. Aguirre-Ollinger, "Exoskeleton control for lower-extremity assistance based on adaptive frequency oscillators: Adaptation of muscle activation and movement frequency," *Proceedings of the Institution of Mechanical Engineers, Part H: Journal of Engineering in Medicine*, vol. 229, no. 1, pp. 52–68, 2015, pMID: 25655955. [Online]. Available: https://doi.org/10.1177/0954411914567213

[8] V. Joukov, V. Bonnet, M. Karg, G. Venture, and D. Kulić, "Rhythmic extended kalman filter for gait rehabilitation motion estimation and segmentation," *IEEE Transactions on Neural Systems and Rehabilitation Engineering*, vol. 26, no. 2, pp. 407–418, 2017.

[9] R. L. Medrano, G. C. Thomas, C. Keais, E. J. Rouse, and R. D. Gregg, "Real-time phase and task estimation for controlling a powered ankle exoskeleton on extremely uneven terrain," *IEEE Trans. Robot.*, 2022, submitted. [Online]. Available: https://web.eecs.umich.edu/locolab/documents/MedranoGregg-TRO2022(submitted).pdf

[10] N. Thatte, T. Shah, and H. Geyer, "Robust and adaptive lower limb prosthesis stance control via extended kalman filter-based gait phase estimation," *IEEE Robotics and Automation Letters*, vol. 4, no. 4, pp. 3129–3136, 2019.

[11] K. R. Embry and R. D. Gregg, "Analysis of continuously varying kinematics for prosthetic leg control applications," *IEEE Transactions on Neural Systems and Rehabilitation Engineering*, pp. 1–1, 2020.

[12] K. R. Embry, D. J. Villarreal, R. L. Macaluso, and R. D. Gregg, "Modeling the kinematics of human locomotion over continuously varying speeds and inclines," *IEEE Transactions on Neural Systems and Rehabilitation Engineering*, vol. 26, no. 12, pp. 2342–2350, 2018.

[13] A. Muniz and J. Nadal, "Application of principal component analysis in vertical ground reaction force to discriminate normal and abnormal gait," *Gait & Posture*, vol. 29, no. 1, pp. 31–35, 2009.

[14] I.-C. Lee, M. M. Pacheco, M. D. Lewek, and H. Huang, "Perceiving amputee gait from biological motion: kinematics cues and effect of experience level," *Scientific Reports*, vol. 10, no. 1, p. 17093, Oct 2020. [Online]. Available: https://doi.org/10.1038/s41598-020-73838-y

[15] P. Federolf, K. Boyer, and T. Andriacchi, "Application of principal component analysis in clinical gait research: Identification of systematic differences between healthy and medial knee-osteoarthritic gait," *Journal of Biomechanics*, vol. 46, no. 13, pp. 2173–2178, 2013.

[16] Y.-Y. Zhang, S.-M. Jiang, Z.-Q. Wei, J.-F. Zhang, and S.-J. Xu, "Individual recognition by gait in virtual space," in *2012 International Conference on Wavelet Analysis and Pattern Recognition*, 2012, pp. 170–174.

[17] K. R. Embry, D. J. Villarreal, R. L. Macaluso, and R. D. Gregg, "The effect of walking incline and speed on human leg kinematics, kinetics, and emg," 2018. [Online]. Available: https://dx.doi.org/10.21227/gk32-e868

[18] H. V. Henderson and S. R. Searle, "The vec-permutation matrix, the vec operator and kronecker products: a review," *Linear and Multilinear Algebra*, vol. 9, no. 4, pp. 271–288, 1981.